Catal Lett (2008) 125:14–21
DOI 10.1007/s10562-008-9523-4

Co_3O_4 and Mn_3O_4 Nanoparticles Dispersed on SBA-15: Efficient Catalysts for Methane Combustion

G. Laugel · J. Arichi · H. Guerba · M. Molière · A. Kiennemann · F. Garin · B. Louis

Received: 22 April 2008 / Accepted: 14 May 2008 / Published online: 3 June 2008

Abstract Co_3O_4 and Mn_3O_4 nanoparticles were successfully impregnated on SBA-15 mesoporous silica. A high dispersion of these metal oxide particles was achieved while using a "two-solvents" procedure, allowing a proper control of the metal oxides loading (7 wt%) and size (10–12 nm). These Co_3O_4 and Mn_3O_4 supported oxides on SBA-15 were characterised by means of XRD, BET and TEM techniques. The influence of the nature of the silica support was investigated in terms of porosity and specific surface area. Since, an improved catalytic activity was achieved over SBA-15 mesoporous silica; it appears that its organised porous meso-structure creates a confinement medium which permits a high dispersion of metal oxide nanoparticles. Supported Co_3O_4/SBA-15 (7 wt%) showed the highest catalytic performance in the combustion of methane under lower explosive limit conditions, comparable to perovskites. These materials become therefore novel efficient combustion catalysts at low metal loading.

Keywords Methane · Catalytic combustion · SBA-15 · Mesopores · Metal oxides

G. Laugel (✉) · J. Arichi · H. Guerba · A. Kiennemann · F. Garin · B. Louis
Laboratoire des Matériaux, Surfaces et Procédés pour la Catalyse, LMSPC—UMR 7515 du CNRS—ECPM—ULP, 25 Rue Becquerel, 67087 Strasbourg, France
e-mail: glaugel@chimie.u-strasbg.fr

H. Guerba
Département de Chimie, Faculté des Sciences, Université Ferhat-Abbas, Setif, Algeria

M. Molière
GE Energy Products—Europe (GEEPE), 20 Avenue du Maréchal Juin, 9007 Belfort Cedex, France

1 Introduction

To avoid risks of explosion in industrial combustion processes, the detection of residual explosive gases, even at low concentration, is warranted [1–3]. Recent reglementations have implemented a sensor response to detect a concentration as low as 5% lower explosive limit (LEL) for methane in the case of gas turbine units. The use of catalytic combustion sensors offers a rapid detection and warning signals [4–6]. These sensors measure the gas concentration as a function of the temperature rise produced by the heat of reaction on the catalytic surface. Therefore, it becomes necessary to develop efficient catalysts for methane complete oxidation at relatively low concentration and temperature (below 600 °C). To fulfill these demanding application constraints, noble metals (Pd, Pt) are well known and highly active for the catalytic combustion of methane [1, 7, 8]. However, these metals exhibit sometimes a poor thermal stability due to sintering or metal volatilization [9, 10]. In comparison, metal oxides M_yO_x (M = Co or Mn) and mixed metal oxides, i.e. perovskites [11–13], pyrochlores [14], offer a valuable alternative with both an improved thermal stability and lower cost.

Bulk metal oxides generally possess a rather low specific surface area (SSA) which seriously hinders their efficiency as catalysts. A convenient way to overcome this drawback is either to impregnate metal oxide nanoparticles on a support, or to disperse them within a porous host having a high SSA. According to their narrow pore size distribution, high SSA and large pore volume, SBA-15 mesoporous silica material is a promising candidate as catalyst support [15–20]. Moreover, SBA-15 possesses a high SSA (600–1,000 m^2/g) and consists in a hexagonal array of uniform tubular channels with tunable pore diameter in the range of 5–30 nm. The synthesis of

SBA-15 material is usually performed using poly(alkylene oxide) tri-block copolymer as surfactant under strong acidic conditions [21], and has attracted great attention in the field of catalysis [22–24]. SBA-15 is therefore one of the most attractive silica host-material for metal or metal oxide nanoparticles.

The operating conditions in the impregnation process of a catalytic phase on a support (precursor, concentration, temperature) strongly influence the structure of its active phase. Conventional procedures to coat oxides remain impregnation and ion exchange techniques. Recently a novel method, so-called "two-solvents" technique, has attracting a considerable interest [25, 26]. This method allows the preparation of highly dispersed metal oxide nanoparticles within silica mesopores, being used as confinement nanoreactors. In a first step, inorganic precursors are introduced into the channels of the mesoporous host. Second, the desired oxide is obtained via an appropriate thermal treatment.

The present study deals with the synthesis and characterisation of Co_3O_4 and Mn_3O_4 nanoparticles selectively grown inside SBA-15 silica support. The catalytic activity of these materials was tested in the combustion of methane at low concentration. The catalytic performance of these materials was compared with perovskite materials, usually considered as one of the most active mixed metal oxide for this reaction [27, 28].

2 Experimental

2.1 Synthesis of SBA-15 Material

The synthesis of SBA-15 material was carried out according to the procedure of Zhao et al. [21]. First, poly(ethylene oxide) poly(propylene oxide) poly(ethylene oxide) ($EO_{20}PO_{70}EO_{20}$, Pluronic P123, BASF) tri-block copolymer was dispersed in an aqueous hydrochloric acid solution ($1 < pH < 2$) under vigorous stirring. After 1 h, a clear solution was obtained indicating a complete dissolution of the surfactant. Then, tetraethyl orthosilicate (TEOS) was added dropwise to the solution at 40 °C under stirring. Gelation and ageing were carried out at 40 °C for 24 h, followed by heating at 100 °C for 72 h in a sealed Teflon flask. The solid was filtered, washed several times with distilled water and dried at room temperature. Finally, the tri-block copolymer template was removed by calcination in air at 500 °C (heating rate 2 °C/min) for 6 h.

2.2 Preparation of the Catalysts

The manganese oxide and cobalt oxide supported catalysts on SBA-15 (Mn_3O_4/SBA-15 and Co_3O_4/SBA-15) were prepared according to the "two-solvents" technique [25]. SBA-15 was at first suspended in dry hexane, used as hydrophobic solvent. Then, a desired amount of metal nitrate (7 or 30 wt%) was dissolved in distilled water, quantity corresponding to the pore volume of SBA-15 determined by N_2 sorption. This aqueous solution containing metal precursors was then added dropwise. The gel was allowed to age for 2 h under vigorous stirring. The solid was recovered by filtration and dried in air. The samples were finally calcined at 700 °C for 6 h (heating rate 2 °C/min) to obtain the desired metal oxides Co_3O_4 and Mn_3O_4. An equimolar loading of Mn and Co oxides on SBA-15 [(Mn–Co)/SBA-15] was prepared following the same procedure. Furthermore, Co_3O_4 metal oxide was also impregnated on silica gel (Grace, US) and zeolite H-Y (Zeochem, Uetikon, Switzerland) for comparison, using the "two-solvents" technique.

$LaCoO_3$ perovskite was prepared according to the resin method from metallo-organic propionate precursors [29, 30]. First, lanthanum and cobalt acetate salts were dissolved in boiling propionic acid. Afterwards, the two solutions were mixed and stirred for 1 h under reflux conditions. Propionic acid was then evaporated until resin formation which hardened upon cooling. This resin was calcined at 700 °C for 4 h (heating rate 3 °C/min) to obtain the desired perovskite crystalline phase.

2.3 Characterisation Techniques

The low-angle powder X-ray diffraction measurements were carried out on a X'PERT MDP apparatus (Philips, Cu Kα radiation) in the theta–theta geometry and associated to a thin film optics, including programmable divergence slit (1/32°), parallel plate collimator, flat Ge monochromator and proportional Xe detector. The system was equipped with TK450 camera of Anton Paar, as sample holder.

The wide angle X-ray diffraction patterns were recorded on a Brucker D8 Advance diffractometer, with a Ni detector side filtered Cu Kα radiation (1.5406 Å) over a 2θ range of 5–90° and a position sensitive detector using a step size of 0.016° and a step time of 7 s.

Nitrogen adsorption–desorption isotherms were measured on a Micromeritics ASAP using nitrogen as gas probe at −96 °C. Before measurement, the sample was outgassed at 300 °C overnight to desorb moisture from the surface. The pore size distribution was determined from the adsorption branch of the isotherm and the SSA values were calculated using the BET model.

Transmission electron microscopy (TEM) measurements were performed on TOPCOM EM 002B microscope for high-magnification (Fig. 1a) and Hitashi S4800 FEG equipped with SE, YAG-BSE and TE detectors (Fig. 1b, c). The samples were dispersed in chloroform and deposited

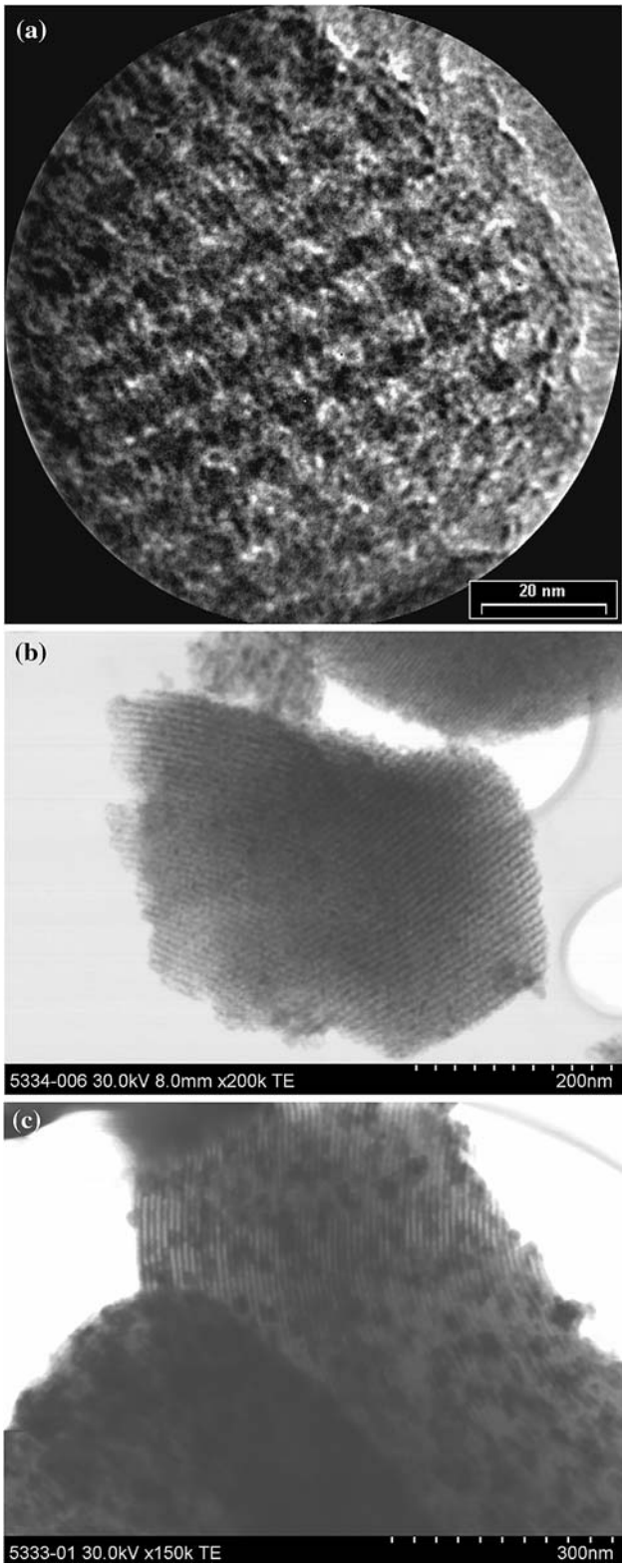

Fig. 1 TEM images of (**a**) Co_3O_4/SBA-15 (7 wt%), (**b**) Mn_3O_4/SBA-15 (7 wt%) and (**c**) Mn_3O_4/SBA-15 (30 wt%)

on a holey carbon film supported on a Cu grid. EDX spectra were acquired to determine the average amount of metal oxides contained in the materials. They were acquired using 20 kV primary electron energy. Quantification was done using the standard-less ZAF correction method in the Genesis software from EDAX.

2.4 Catalytic Tests

The catalytic combustion of methane was performed under air in a fixed-bed reactor at atmospheric pressure. The quartz reactor is a U-shaped tube of 5 mm of inner diameter. The catalyst (150 mg) was packed between quartz wool plugs and placed in the middle part of the reactor. The void part of the reactor was filled by inert quartz pellets. The total gas flow of methane and air was set to 3 L/h, regulated by means of mass flow controllers (MFC, Brooks 5850 TR series). The concentration of methane was set to 5% of its LEL, i.e. 2,500 ppm. The activity of the catalysts was tested between 300 and 650 °C the temperature was kept constant during 45 min at each step (each 50 °C). The composition of the gas flow at the reactor outlet was analysed on-line by means of a Micro-GC 3000 gas analyzer (Agilent Technologies). A TCD detector was used for the Micro-GC which is composed by three modules with Porapack U (PPU), methylpolysiloxane (OV1) and Molecular sieve 5 Å (MS5A) columns.

3 Results and Discussion

3.1 Characterisations of Co_3O_4/SBA-15 and Mn_3O_4/SBA-15 Catalysts

The structures of synthesised Co_3O_4 and Mn_3O_4 in SBA-15 mesopores, 7% in weight, have been first examined by powder XRD, and the profiles are depicted in Figs. 2 and 3. Figure 2 presents the low-angle diffraction patterns of bare SBA-15, Co_3O_4/SBA-15 (7 wt%) and Mn_3O_4/SBA-15 (7 wt%) samples. Three well-resolved peaks are detected for bare SBA-15 (Fig. 2a). These reflexions can be indexed to the (1 0 0), (1 1 0) and (2 0 0) diffractions of the ordered *p6mm* hexagonal space group [21]. It is noteworthy that only the (1 0 0) reflexion is still observed for Co_3O_4/SBA-15 (7 wt%) and Mn_3O_4/SBA-15 (7 wt%) materials (Fig. 2b, c). The incorporation of nanoparticles of metal oxides contributes to the drastic intensity decrease for Co_3O_4/SBA-15 (7 wt%) and Mn_3O_4/SBA-15 (7 wt%) (1 0 0) diffraction peak (Fig. 2b, c). This phenomenon was already observed by several authors [31, 32]. Figure 3a confirms

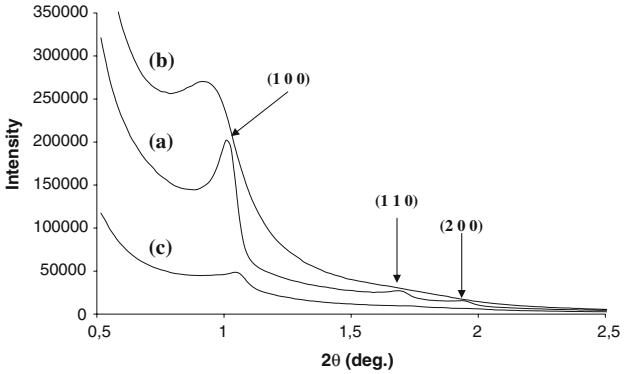

Fig. 2 Low-angle XRD patterns of (**a**) SBA-15, (**b**) Mn_3O_4/SBA-15 (7 wt%) and (**c**) Co_3O_4/SBA-15 (7 wt%)

the formation of crystallised Co_3O_4 cobalt oxide (JCPDS 065-3103). The broad peak between $10° \leq 2\theta \leq 30°$ corresponds to the mesoporous silica. The size of the nanoparticles was calculated using the Debye–Scherrer formula from the full width at half maximum (FWHM) of the (4 0 0) diffraction. A size of 11 ± 2 nm was estimated for Co_3O_4 nanoparticles. According to Geus and coworkers [33] the stable manganese oxide phases in air at 750 °C are either Mn_2O_3 or Mn_3O_4. The indexation of the different reflections shown by the wide-angle diffraction pattern (Fig. 3b), clearly evidenced exclusive the formation of Hausmannite Mn_3O_4 cristalline phase (JCPDS 080-0382) [34]. The particle size was calculated to be 10 ± 2 nm from the FWHM of the (2 2 0) diffraction peak of Mn_3O_4.

The nitrogen adsorption–desorption isotherms of bare SBA-15 and Co_3O_4/SBA-15 are displayed in Fig. 4. The isotherm of siliceous SBA-15 (Fig. 4a) exhibits a type IV isotherm with H1 hysteresis following the IUPAC classification [35]. This profile is a characteristic of mesoporous materials having one-dimensional cylindrical channels. A sharp inflection in the relative pressure (P/P_0) between 0.6 and 0.8 corresponds to capillary condensation within uniform mesopores and is a function of the pore diameter. The uniform pore size distribution is demonstrated by the sharpness of this step and displayed in Fig. 4b. The isotherm of the Co_3O_4/SBA-15 (7 wt%) sample (Fig. 4c) also shows the typical profile of pristine SBA-15. However, the sharp inflection shifts toward lower pressures, suggesting that metal oxide (Co_3O_4) nanoparticles are present within SBA-15 mesopores. Both pore diameters and SSA were decreased from 6.8 to 5.6 nm, and from 785 to 338 m^2/g for pristine SBA-15 and Co_3O_4/SBA-15 (7 wt%), respectively. It is important to note that the mesoporous structure was preserved after the catalytic runs. Similar results were obtained for Mn_3O_4/SBA-15 (7 wt%) sample: pore diameter = 5.2 nm and SSA = 316 m^2/g.

High-magnification TEM image (Fig. 1a) evidences the hexagonal arrangement of the porous network after Co_3O_4 impregnation. Mn_3O_4/SBA-15 microstructure was further investigated by TEM (Fig. 1b, c). Obviously, SBA-15 with a lower quantity of manganese oxide (7 wt%) shows a homogeneous and high dispersion of nanoparticles formed exclusively within mesoporous channels (Fig. 1b). In contrast, SBA-15 having a higher manganese oxide loading (30 wt%) presents larger aggregates (Fig. 1c). Despite uncertainties in the particle size, observed by TEM, due to changes in electron density [26], sizes of metal oxide nanoparticles (Mn_3O_4 and Co_3O_4) are consistent with the values calculated with Debye–Scherrer formula, i.e. 11 and 10 ± 2 nm for Co_3O_4 and Mn_3O_4, respectively.

EDAX analysis confirmed the presence of Co and Mn elements in the SBA-15 at the desired loadings. An average content of metal of 6.7 and 7.2 wt% was determined for Co_3O_4/SBA-15 (7 wt%) and Mn_3O_4/SBA-15 (7 wt%), respectively. Again, the efficiency of the "two-solvents"

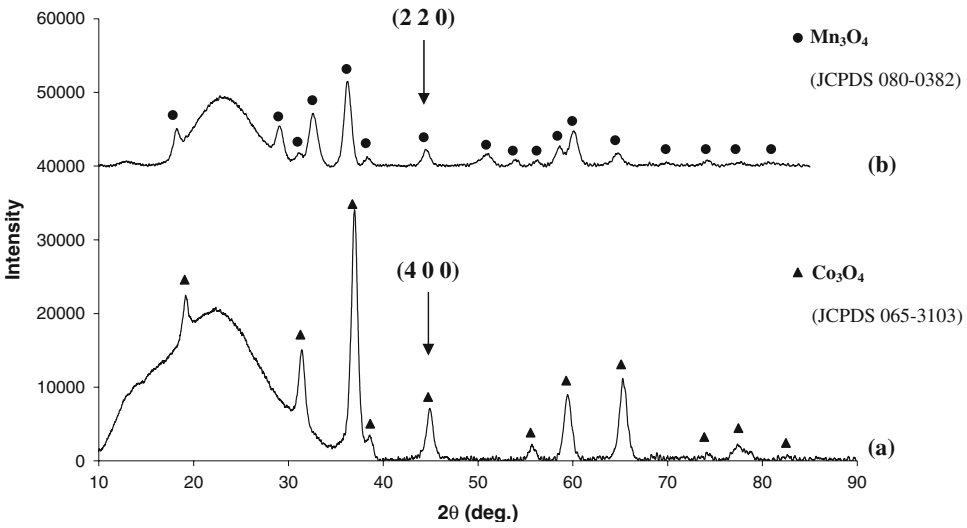

Fig. 3 XRD patterns at wide angle of (**a**) Co_3O_4 and (**b**) Mn_3O_4 nanoparticles supported on SBA-15

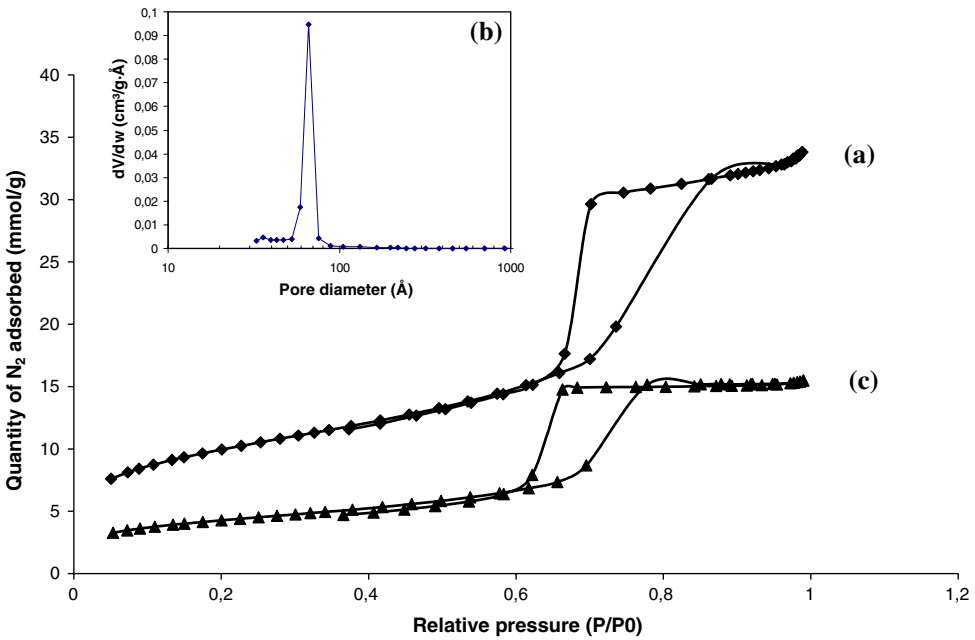

Fig. 4 (**a**) Nitrogen adsorption–desorption isotherm of SBA-15, (**b**) pore size distribution of SBA-15 and (**c**) nitrogen adsorption–desorption isotherm of Co_3O_4/SBA-15 (7 wt%)

method is confirmed for the impregnation of nanoparticles having both controlled size and loading.

3.2 Catalytic Activity

3.2.1 Activity in Methane Total Oxidation

The activity in methane complete oxidation was expressed in terms of CH_4 conversion with respect to the reaction temperature for Co_3O_4 and Mn_3O_4 supported on SBA-15 at different loadings, and $LaCoO_3$ perovskite. The temperatures of 50% (T_{50}) and 90% (T_{90}) methane conversion were used to compare the activity of the catalysts (Table 1). Figure 5 shows the dependence between CH_4 conversion and the reaction temperature for 7 and 30 wt% supported manganese oxides, and 7 wt% supported cobalt oxide. As a comparison, 7 wt% of supported mixed manganese–cobalt oxide (equimolar) was also tested. It is noteworthy that a higher loading of manganese oxide (30 wt%) led to a decrease in the rate of CH_4 conversion when compared to 7 wt% catalysts. The T_{50} temperature was reached 18 °C below for Mn_3O_4/SBA-15 (7 wt%) than for the 30 wt% material. This difference was further increased to 27 °C for T_{90} values (Table 1). According to TEM images (Fig. 1), manganese oxide tends to form large aggregates at high loading (30 wt%). A lower loading of active phase on SBA-15 insures therefore a homogeneous dispersion of nanoparticles within the mesoporous silica channels, and thus allow an improved catalytic activity. Supported cobalt oxide on SBA-15 (7 wt%) exhibits the highest catalytic activity in the methane oxidation when compared to manganese oxide-based catalyst. These results are in line with those generally reported for total oxidation of hydrocarbons: $Co_3O_4 > Mn_3O_4 > Cr_2O_3 > CuO$ [10, 36–39]. It is interesting to note that the differences in the T_{50} between Co_3O_4/SBA-15 and Mn_3O_4/SBA-15 are less pronounced at T_{90}, i.e. at high temperatures (>570 °C). Thus the same conversion obtained for all catalysts at high temperature is mainly due to the thermodynamic effect.

At temperatures below 550 °C, Co_3O_4/SBA-15 exhibits the highest methane conversion. Whereas at temperature above 550 °C, a rapid increase in activity of Mn_3O_4/SBA-15 catalyst was observed, thus leading to the narrowing in the difference in methane conversion efficiency among Co_3O_4/SBA-15 and Mn_3O_4/SBA-15 catalysts. Such change in the catalyst behaviour with respect to the temperature can be interpreted, as suggested by many authors for metal oxides, in terms of a change in methane total oxidation mechanism [40–43]. Indeed, efficient catalysts for methane complete oxidation must provide a high rate of molecular oxygen activation [40]. These materials are therefore characterised by a large number of active sites which can coordinate an oxygen molecule, hence being able to easily donate and accept electrons. Metal oxides having an unfilled d-shell exhibit these properties. Furthermore, the protagonists should also provide a slow transformation of active oxygen into lattice oxygen [36]. At low temperature, the rate-determining step of complete oxidation reaction is generally the decomposition of oxidised surface species. The activity of metal oxides in deep oxidation process depends on oxygen mobility, in other words, in the strength of metal–oxygen bonds [40, 42]. The strength of M–O bond inhibits its O-lability, hence reduces the activity of this oxide [36]. This suggests that oxidation catalysts can

Table 1 T_{50} and T_{90} temperatures for the different catalysts

	T_{50} temperature (°C)	T_{90} temperature (°C)	SSA (m^2/g)	Metal contents (%)
Co_3O_4/SBA-15 (7 wt%)	506	576	338	6.7
Mn_3O_4/SBA-15 (7 wt%)	534	588	327	7.2
Mn_3O_4/SBA-15 (30 wt%)	552	615	295	28
(Mn–Co)/SBA-15 (7 wt%)	541	589	322	3.2 (Mn)/3.5 (Co)
$LaCoO_3$	514	591	11	–
Co_3O_4/SiO_2 (7 wt%)	545	605	185	6.8
Co_3O_4/Zeo H-Y (7 wt%)	552	614	383	7.3

be classified as a function of the stability of the oxide. The enthalpy of metal–oxygen bond formation ($\Delta H°_{298}$) is 105 kJ/mol higher for Mn than for Co. It appears therefore that manganese forms more stable oxides than cobalt [41]. We can therefore argue that the differences in temperature lower than 550 °C between Co_3O_4/SBA-15 and Mn_3O_4/SBA-15 can be rationalised on a basis of the stability of their M–O bond. In term of methane activation, a relatively weak M–O bond, i.e. less stable metal oxide, favours an important interaction between the metal catalyst and gaseous methane, leading to an ease of methane activation. Consequently, Co_3O_4/SBA-15 is more efficient than Mn_3O_4/SBA-15. Nevertheless, at temperature above 550 °C, the reaction rate becomes independent to the nature of the interaction between the oxidised reactant and the catalyst. This tends to draw nearer the light-off curves of the two catalysts.

An equimolar loading of Mn and Co oxides (7 wt%) on SBA-15 was also tested in the conversion of methane into carbon dioxide. From the light-off curves (Fig. 5), the (Mn–Co)/SBA-15 mixed catalyst exhibits a lower activity when compared to both Co_3O_4/SBA-15 and Mn_3O_4/SBA-15. Such inhibitor effect of supported bimetallic Co and Mn oxides, in terms of T_{50}, has already been observed by Li et al. in the combustion of methane [22].

Perovskite type oxides (ABO_3) are particularly promising catalysts in the combustion of hydrocarbons owing to their high thermal stability and important oxygen mobility within the crystal lattice [13, 44]. High catalytic activities in methane combustion over $LaBO_3$ (B = Co or Mn) were reported by Arai et al. [11]. We have therefore performed a comparison with $LaCoO_3$ perovskite (SSA = 11 m^2/g) under the same conditions, i.e. 150 mg of catalyst and with the same catalyst bed length ($LaCoO_3$ diluted in SiO_2). Figure 6 shows light-off curves of Co_3O_4/SBA-15 (7 wt%), Mn_3O_4/SBA-15 (7 wt%) and $LaCoO_3$. It is seen that Co-oxide nanoparticules impregnated on SBA-15 exhibit relatively same catalytic activity than Co-based perovskite. A homogeneous dispersion of metal oxide nanoparticles within the channels of the mesoporous SBA-15 provides a confined active site, able to adsorb, and thus activate methane efficiently on different crystallite faces [40]. The mesoporous structure is maintained after the catalytic run, since both the hysteresis loop and the SSA values were preserved for Co_3O_4/SBA-15 (7 wt%) and Mn_3O_4/SBA-15 (7 wt%) (not presented here).

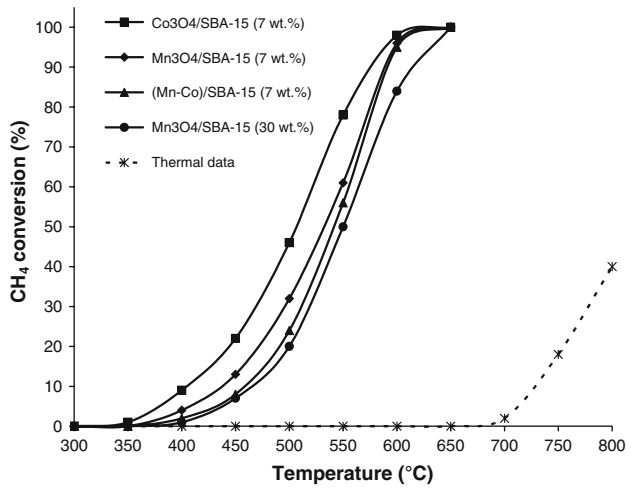

Fig. 5 Methane conversion as a function of temperature for manganese and cobalt oxides supported on SBA-15

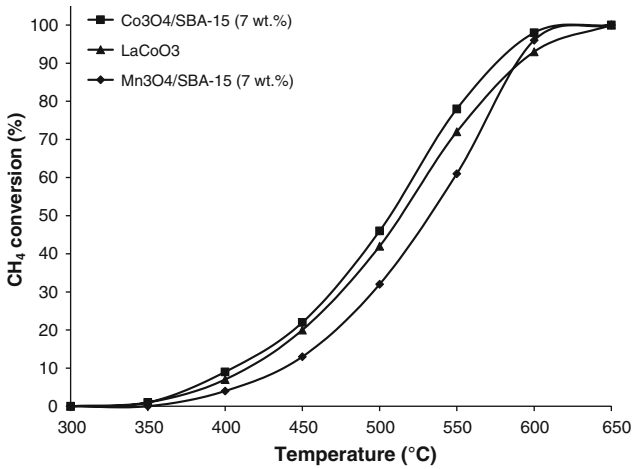

Fig. 6 Comparison between supported metal oxides on SBA-15 and $LaCoO_3$ perovskite

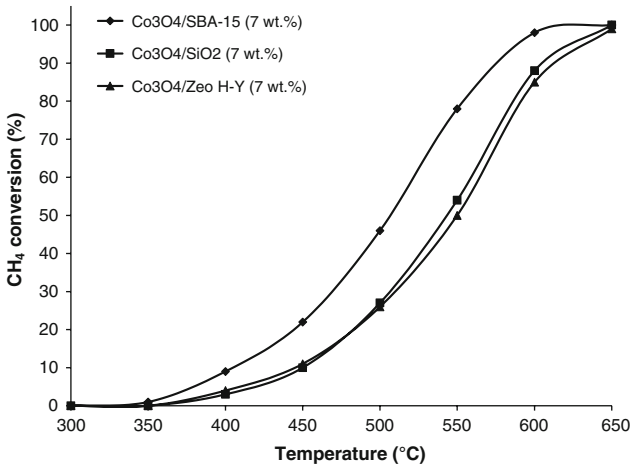

Fig. 7 Influence of the nature of the silica support on methane catalytic combustion

3.2.2 Influence of the Support in Methane Conversion

Figure 7 shows the conversion of methane over cobalt oxide Co_3O_4 (7 wt%) loaded on different supports: SBA-15, silica gel, and zeolite H-Y with SSA equal to 785, 300 and 600 m^2/g, respectively. Surprisingly, the activity of the Co_3O_4/Zeo H-Y (7 wt%) catalyst was similar to Co_3O_4/SiO_2 (7 wt%) in spite of its higher SSA value. Again, Co_3O_4/SBA-15 (7 wt%) presented the highest catalytic activity. Mass transfer are known to be hindered within the zeolite micropores [45]. On the contrary, mesoporous silica SBA-15 offers sufficient space to allow a rapid diffusion of reactant/product in a confined environment.

4 Conclusions

In summary, Co_3O_4 and Mn_3O_4 nanoparticles were highly dispersed within SBA-15 silica channels, while using a "two-solvents" procedure, i.e. one being hydrophilic, the other hydrophobic. The synthesis procedure allowed a proper control of both the size and the loading of these metal oxides.

Co_3O_4/SBA-15 (7 wt%) exhibited the highest catalytic performance in the conversion of methane to carbon dioxide and water even, at 5% of LEL concentration. This opens up a novel route to produce efficient combustion catalysts, without Pd-use and at low metal loading.

Thanks to its mesoporous structure, SBA-15 seems to present the appropriate pore architecture and size to ensure a high and homogeneous dispersion of Mn_3O_4 and Co_3O_4 oxides, thus creating a confinement media, being resistant to sintering.

Acknowledgments The authors would like to thank GE Energy Products—Europe for financial support (GL). Dr. B. Heinrich (GMO-IPCMS, France), S. Libs, and C. Hulot are gratefully acknowledged for technical assistance.

References

1. Gelin P, Primet M (2002) Appl Catal B 39:1
2. Moliere M, Cozzarin P, Bouchet S, Rech P (June 6-9 2005) ASME Turbo Expo 2005, Reno
3. Molière M, Cozzarin P, Bouchet S, Rech P (May 8-11 2006) ASME Turbo Expo 2006, Barcelona, Spain
4. Gentry SJ, Jones TA (1986) Sens Actuators 10:141
5. Han C-H, Hong D-W, Han S-D, Gwak J, Singh KC (2007) Sens Actuators 125:224
6. Lundstrom I (1996) Sens Actuators B 35:11
7. Ciuparu D, Lyubovsky MR, Altman E, Pfefferle LD, Datye A (2002) Catal Rev-Sci Eng 44:593
8. Ozawa Y, Tochihara Y, Mori N, Yuri I, Sato J, Kagawa K (2003) Catal Today 83:247
9. Spivey JJ, Butt JB (1992) Catal Today 11:465
10. Zwinkels MFM, Järås SG, Menon PG (1993) Catal Rev-Sci Eng 35:319
11. Arai H, Yamada T, Eguchi K, Seiyama T (1986) Appl Catal 26:265
12. McCarty JC, Wise H (1990) Catal Today 8:231
13. Pena MA, Fierro JLG (2001) Chem Rev 101:1981
14. Sohn JM, Kim MR, Woo SI (2003) Catal Today 83:289
15. Corma A, Kumar D (1998) Stud Surf Sci Catal 117:201
16. El Berrichi Z, Louis B, Tessonnier JP, Ersen O, Cherif L, Ledoux MJ, Pham-Huu C (2007) Appl Catal A 316:219
17. Louis B, Subrahmanyam C, Kiwi-Minsker L, Viswanathan B, Buffat PA, Renken A (2002) Catal Commun 3:159
18. Rivera-Muñoz E, Lardizabal D, Alonso G, Aguilar A, Siadati MH, Chianelli RR (2003) Catal Lett 85:147
19. Taguchi A, Schuth F (2005) Micropor Mesopor Mater 77:1
20. Vradman L, Landau MV, Herskowitz M, Ezersky V, Talianker M, Nikitenko S, Koltypin Y, Gedanken A (2003) J Catal 213:163
21. Zhao D, Feng J, Huo Q, Melosh N, Fredrickson GH, Chmelka BF, Stucky GD (1998) Science 279:548
22. Cao Y, Hu J-C, Yang P, Dai W-L, Fan K-N (2003) Chem Commun: 908
23. Dufaud V, Davis ME (2003) J Am Chem Soc 125:9403
24. Fornes V, Lopez C, Lopez HH, Martinez A (2003) Appl Catal A 249:345
25. Imperor-Clerc M, Bazin D, Appay MD, Beaunier P, Davidson A (2004) Chem Mater 16:1813
26. Lopes I, ElHassan N, Guerba H, Wallez G, Davidson A (2006) Chem Mater 18:5826
27. Alifanti M, Kirchnerova J, Delmon B, Klvana D (2004) Appl Catal A 262:167
28. Choudhary TV, Banerjee S, Choudhary VR (2002) Appl Catal A 234:1
29. Sinquin G, Petit C, Hindermann JP, Kiennemann A (2001) Catal Today 70:183
30. Rehspringer JL, Bernier JC (1986) Mat Rec Soc Symp Proc 72:67
31. Tian B, Liu X, Yang H, Xie S, Yu C, Tu B, Zhao D (2003) Adv Mater 15:1370
32. Han Y-F, Chen F, Ramesh K, Zhong Z, Widjaja E, Chen L (2007) Appl Catal B 76:227
33. Stobbe ER, de Boer BA, Geus JW (1999) Catal Today 47:161
34. Escax V, Imperor-Clerc M, Bazin D, Davidson A (2005) C R Chimie 8:663
35. Sing KSW, Everett DH, Haul RAW, Mosenu L, Pierotti RA, Rouquerol J, Siemieniewska T (1985) Pure Appl Chem 57:603
36. O'Connell M, Norman AK, Huttermann CF, Morris MA (1999) Catal Today 47:123

37. Torncrona A, Skoglundh M, Thormahlen P, Fridell E, Jobson E (1997) Appl Catal B 14:131
38. Yu Yao YF (1974) J Catal 33:108
39. Yu Yao YF (1975) J Catal 39:104
40. Sokolovskii VD (1990) Catal Rev-Sci Eng 32:1
41. Spivey JJ (1987) Ind Eng Chem Res 26:2165
42. Yuranov I, Dunand N, Kiwi-Minsker L, Renken A (2002) Appl Catal B 36:183
43. Yuranov I, Kiwi-Minsker L, Renken A (2003) Appl Catal B 43:217
44. Tejuca LG, Fierro JLG, Tascon JMD (1989) Adv Catal 36:237
45. Louis B, Kiwi-Minsker L, Reuse P, Renken A (2001) Ind Eng Chem Res 40:1454